frontiers | Frontiers in Chemical Engineering

TYPE Original Research
PUBLISHED 23 January 2023
DOI 10.3389/fceng.2022.1116366

OPEN ACCESS

EDITED BY
Jose M. Campos-Martín,
Institute of Catalysis and Petrochemistry (CSIC), Spain

REVIEWED BY
Hongyang Liu,
Institute of Metal Research (CAS), China
Ying Li,
Zhejiang University of Technology, China

*CORRESPONDENCE
Jingjie Luo,
jingjie.luo@dlut.edu.cn
Changhai Liang,
changhai@dlut.edu.cn

SPECIALTY SECTION
This article was submitted to Catalytic Engineering, a section of the journal Frontiers in Chemical Engineering

RECEIVED 05 December 2022
ACCEPTED 28 December 2022
PUBLISHED 23 January 2023

CITATION
Du Z, Zhang S, Yang S, Yang W, Luo J and Liang C (2023), Promotion of Au nanoparticles on carbon frameworks for alkali-free aerobic oxidation of benzyl alcohol.
Front. Chem. Eng. 4:1116366.
doi: 10.3389/fceng.2022.1116366

Promotion of Au nanoparticles on carbon frameworks for alkali-free aerobic oxidation of benzyl alcohol

Zhongtian Du, Sen Zhang, Sihan Yang, Wenhao Yang, Jingjie Luo* and Changhai Liang*

State Key Laboratory of Fine & Chemicals, Laboratory of Advanced Materials & Catalytic Engineering, School of Chemical Engineering, Dalian University of Technology, Panjin, China

We synthesized a series of modified Co-ZIF-67 materials with tunable morphology to support fine Au nanoparticles for the alkali-free aerobic oxidation of benzyl alcohol. Structure promotion was performed using Stöber silica as a hard template, which was subsequently removed by NaOH etching before gold immobilization. The texture structure of Au/(Si)C was greatly improved with increasing surface area and volume. CoO_x was simultaneously introduced into the carbon shell from the Co-ZIF-67 precursor, which consequently facilitated the specific Au-support interaction *via* bimetallic synergy. XRD, XPS, and TEM images demonstrated the redispersion of both Au and CoO_x as well as the electronic delivery between metals. Analysis of the chemical and surface composition suggested a surface rich in $Au^{\delta+}$ with abundant lattice oxygen contributed by CoO_x in the final Au/(Si)C, which improved the transformation rate of benzyl alcohol even in an alkali-free condition. Au/(Si)C with finely dispersed Au particles showed excellent catalytic performance in the alkali-free environment, with 89.3% benzyl conversion and 74.5% benzaldehyde yield under very mild conditions.

KEYWORDS

benzyl alcohol, alkali-free oxidation, Au/C-CoOx, ZIF-67, benzaldehyde

1 Introduction

Benzaldehyde (BzH) has long been used in the chemical industry as an important fine chemical and intermediate (Guo et al., 2014). It plays an important role in our daily lives and is often used in the production of medical treatments, dyes, spices, resins, etc. (Cánepa et al., 2017). Studies in recent years have reported the transformation of benzyl alcohol (BnOH) to benzaldehyde by selective oxidation using molecular oxygen to avoid the production of toxic substances, with pure oxygen or even air used as oxidants under environmental-friendly conditions, thus meeting the concept of green chemistry (Feng et al., 2015; Tang et al., 2019).

In recent years, noble metal catalysts have attracted attention due to their high catalytic performances in a variety of heterogeneous reactions (Chen et al., 2021; Jia et al., 2022). Among them, Au catalysts have shown outstanding efficiency for the selective oxidation of primary alcohols compared to other noble metals, although mostly in the presence of an additional alkali (Yu et al., 2013; Adnan and Golovko, 2019). Ferraz et al. (2016) reported the use of different basic promoters to enhance the catalytic activity of Au/TiO_2 for the selective oxidation of benzyl alcohol. The presence of K_2CO_3 was indispensable for increasing BnOH conversion from 2% to 72%. The addition of alkali leads to challenges including environmental pollution and equipment corrosion, which hinder the use of Au catalysts in industrial-scale development.

To adapt to the demand for alkali-free processes, researchers have reported promotion strategies using basic metal oxides as supports or dopants; e.g., CeO_2, MgO, NiO, and CoO_x (Wang et al., 2015;

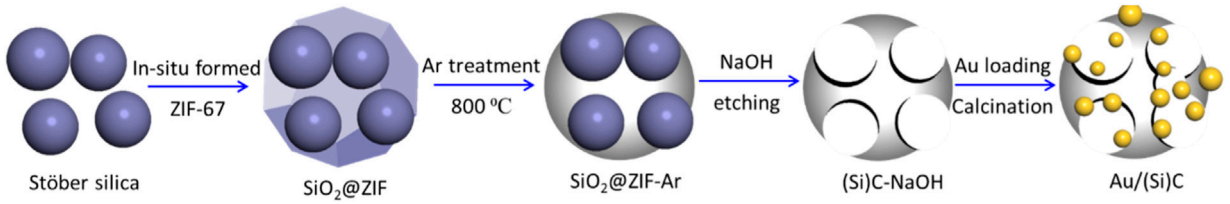

SCHEME 1
Schematic illustration of sample preparation. Stöber silica was synthesized in the lab by reacting $NH_3{\cdot}H_2O$ and TEOS in ethanol.

Parmeggiani et al., 2017). The density of surface alkalinity can be tuned to benefit the fracture of C-H bonds with improved oxidation behavior for primary alcohols (Chen et al., 2010). Su et al. (2008) prepared a series of binary mesomorphic $Ga_xAl_{6-x}O_9$ solid solutions to support Au nanoparticles, which facilitated the oxidation of benzyl alcohol without any external alkali source. Xu et al. (2020) synthesized an Ni_3Al-LDH support to anchor small gold clusters *via* electrostatic adsorption and specific basicity for alkali-free oxidation.

In a previous study, we used carbon-supported gold nanoparticles in a colloid immobilization method (Luo et al., 2022a; Luo et al., 2022b). Our results showed that the surface of carbon materials could be easily tuned by introducing hetero-atoms, which provided rapid reaction rates and stability under appropriately designed surfaces and structures. However, the Au/C-based catalysts required the presence of a strong base such as NaOH or Na_2CO_3 to act as a proton acceptor for alcohol oxidation, although the carbon supports showed superiority with large reserves and controllable micro-surfaces. As an alternative, metal-organic frameworks (MOFs) have attracted interest in recent decades, in which a basic metal (oxide) can be confined in carbon layers (Lu et al., 2022), thus providing more possibilities for metal-modulated carbons as promising supports for gold in the alkali-free oxidation of primary alcohols. Zhu et al. (2014) prepared a Zr-MOF-coated Au/UIO-66 catalyst, which showed a 53.7% benzaldehyde yield at 80 °C. Liu et al. (2018) also suggested that the unique micro reactor type structure in Ag@Au/ZIF-8 improved AuNP dispersion and the reactant adsorption speed, revealing the advantages of MOF precursors.

Herein, we propose a new strategy to synthesize CoO_x-doped carbon-supported Au nanoparticles with structure promotion. Co-ZIF-67 was synthesized in the presence of Stöber silica to obtain carbon layer-encapsulated silica spheres. A well-developed mesoporous structure was obtained after NaOH etching. The resulting abundant-mesoporous carbon material could be used as an efficient support for gold nanoparticles, which displayed surprisingly high alkali-free activity for benzyl alcohol oxidation under very mild conditions (80 °C, atmospheric pressure). Characterization, including XRD, XPS, SEM, TEM, and N_2 adsorption-desorption, was performed for an in-depth understanding of the influences of the promoted structure and the chemical composition.

2 Experimental section

2.1 Material synthesis

Cobalt nitrate (II) ($Co(NO_3)_2{\cdot}6H_2O$), tetraethyl orthosilicate (TEOS), 2-methylimidazole (HMIM, $C_4H_6N_2$), ethanol, ammonia, benzyl alcohol, chloroauric acid ($HAuCl_4$), sodium borohydride ($NaBH_4$), and NaOH were purchased from China National Pharmaceutical Group Corporation. All chemicals (analytical grade) were used as received without further purification.

2.2 Catalyst synthesis

The typical synthesis of a promoted gold catalyst is illustrated in Scheme 1.

2.2.1 Stöber silica

Stöber silica was synthesized using the Stöber method as described previously (Luo et al., 2013). A mixed solution of TEOS and EtOH (volume ratio of 1:5) was added to a 250 mL baker. H_2O and $NH_3{\cdot}H_2O$ were homogeneously mixed with EtOH and injected into the above baker. The initial volume ratio of $TEOS{:}H_2O{:}NH_3{\cdot}H_2O{:}EtOH$ was fixed at 5:1:5:100. After stirring at room temperature for 16 h, the solution was *in situ* dried in the baker at 60 °C to obtain a dry powder. Stöber silica consisting of spherical silica balls approximately 90 nm in diameter was obtained, which was washed and filtered in distilled water and ethanol to remove all residual organic compounds. For comparison, Stöber silica with an average diameter of approximately 350 nm was also synthesized with a $TEOS{:}H_2O{:}NH_3{\cdot}H_2O{:}EtOH$ fixed ratio of 5:10:5:100.

2.2.2 SiO_2@ZIF

SiO_2@ZIF was synthesized in the presence of Stöber silica spheres. In this process, 1 g of silica powder was mixed with 2-methylimidazole in distilled water and sonicated for 30 min. Cobalt nitrate (II) was slowly added dropwise to the above mother solution with stirring. The atomic ratio between $2\text{-methylimidazole:Co:}SiO_2{:}H_2O$ was 40:1:3:220. The color of the above solution changed to purple and was stirred for 12 h at room temperature. After washing four times in distilled water and drying in an oven at 60 °C, the resulting SiO_2@ZIF powder was ground.

2.2.3 Thermal treatment and etching of SiO_2@ZIF

The SiO_2@ZIF was thermally treated in Ar at 800 °C at a heating rate of 2 °C/min and maintained for 5 h to obtain SiO_2@ZIF-Ar. The silica was subsequently etched and removed using a 2.0 mol/L NaOH solution for 12 h. The resulting gray deposition was washed and filtered until the pH was neutral; (Si)C-NaOH was produced after drying to assess the carbon support with an etched silica core.

2.2.4 Au/(Si)C

Au/(Si)C was prepared by the colloid immobilization method using the pre-treated (Si)C-NaOH support. An aqueous solution of

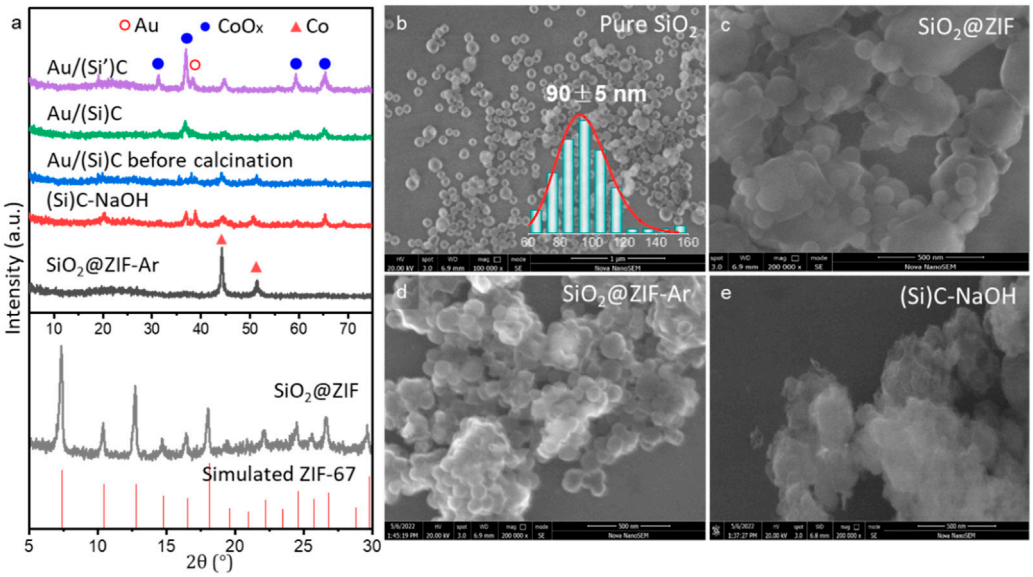

FIGURE 1
(A) XRD patterns and **(B–E)** SEM images of different samples during synthesis. Au/(Si')C was synthesized using a similar method as that for Au/(Si)C, but based on silica with larger spheres (350 nm).

$HAucl_4{\cdot}3H_2O$ (5.1×10^{-2} mol/L) was mixed with 0.1 g/L PVA solution for 30 min (weight ratio of PVA/Au/H_2O of 5:1:65). The pre-treated (Si)C-NaOH was subsequently added to the mixture with Au loading at 1.5 wt%. A fresh $NaBH_4$ (0.1 mol/L) solution was rapidly added to the solution (molar ratio of $NaBH_4$/Au of 5:1); the resulting wine-red solution suggested the formation of a fine gold colloid. The solution was further stirred for 12 h, during which time the supernatant became colorless, indicating the full loading of colloidal Au particles. After washing, filtration, and drying at 60 °C overnight, an Au/CS powder was obtained and calcined in air at 300 °C for 3 h to obtain the final Au/(Si)C. For comparison, another Au/(Si')C sample was prepared using Stöber silica with large spheres (350 nm), which were synthesized as described in Section 2.2.1.

2.3 Characterization

N_2 adsorption-desorption was analyzed on a Micromerit-ics ASAP 2020 device (United States) in liquid nitrogen at 77 K. Powder X-ray diffraction (XRD) patterns were recorded on a Lab XRD-7000s with graphite-monochromatized Cu Kα radiation at a scanning rate of 5°/min over a 2θ range from 5° to 80°. TEM images were obtained at 200 kV on a Tecnai G2-F30 TWIN instrument. SEM images were obtained on a Nova Nano SEM 450 scanning electron microscope to determine the catalyst morphology and microstructure. XPS spectra were obtained using an ESCALab220i-XL electron spectrometer (VG Scientific) using 300 W Al-K radiation. Raman spectra were collected on a Raman spectrometer (JY, HR 800) using a 514 nm laser.

2.4 Catalytic performance

The catalytic performances of different catalysts for alkali-free oxidation of benzyl alcohol were measured in the absence of alkali. A mixture of 0.054 g benzyl alcohol, 15 mg catalyst, and 8 ml paraxylene was added to a 25 ml three-necked flask. The flask was placed in an oil bath with a reflux condenser. Oxygen was continuously flowed into the flask at 20 ml/min. After reacting for several hours, the solution was cooled to room temperature and analyzed on a gas chromatograph (Agilent GC-7890) using paraxylene as the reference substance. The conversion of benzyl alcohol ($Conv._{BnOH}$) and the selectivity for benzaldehyde ($Sel._{BzH}$) were calculated as follows:

$$Conv._{BnOH}(\%) = \frac{C_0 - C_{BnOH}}{C_0} \times 100\%$$

$$Sel._{BzH}(\%) = \frac{C_0 - C_{BnOH}}{C_0} \times 100\% Sel._{BzH}(\%)$$

$$= [C_{BzH}/(C_0 - C_{BnOH})] \times 100$$

where C_0, C_{BnOH}, and C_{BzH} are the initial concentration of benzyl alcohol and the final concentrations of benzyl alcohol and benzaldehyde, respectively.

3 Results and discussion

In this work, a new type of carbon material–supported Au catalyst with promoted structure was synthesized, as illustrated in Scheme 1. The XRD patterns of typical samples during the synthesis of Au/(Si)C are shown in Figure 1A. Silica was synthesized by the Stöber method and used as a hard template with monodispersed spheres approximately 90 nm in diameter (Figure 1B) according to previous work (Luo et al., 2013).

The SiO_2@ZIF sample synthesized in the presence of silica presented XRD patterns similar to those for the simulated ZIF-67 phase, suggesting the successful formation of the ZIF-67 structure (Zhou et al., 2020). After thermal treatment in Ar at 800 °C, most of the diffraction peaks disappeared in the SiO_2@ZIF-Ar, and two additional

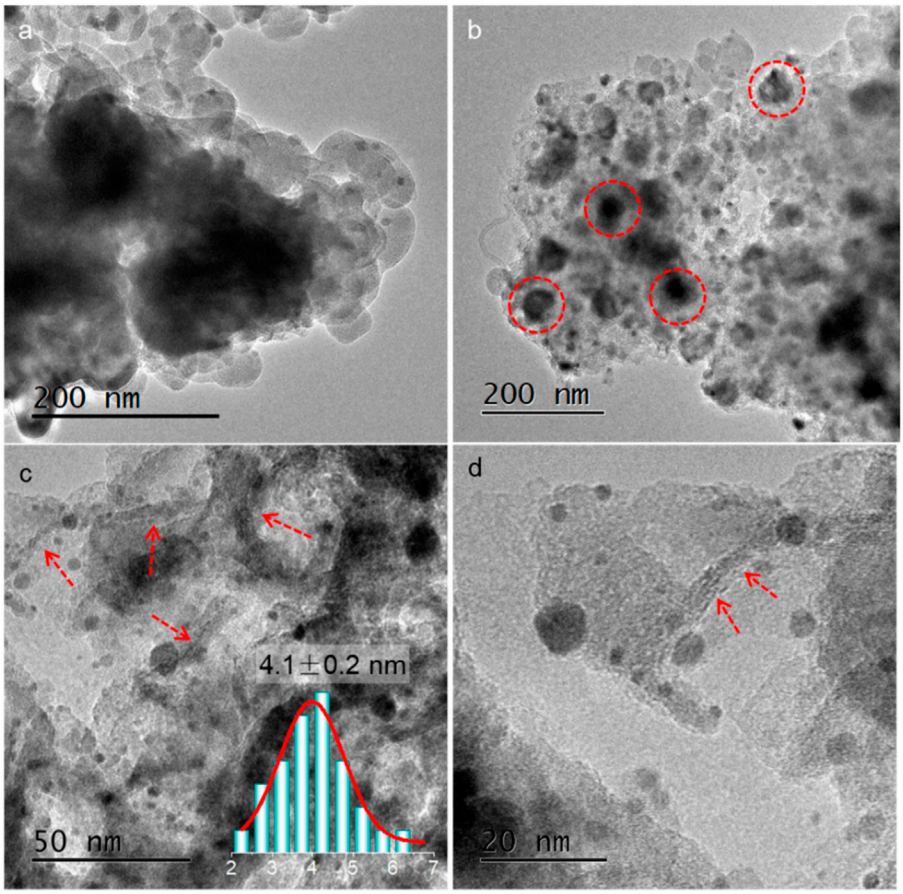

FIGURE 2
TEM images of **(A)** SiO_2@ZIF-Ar after Ar thermal treatment, **(B)** (Si)C-NaOH after NaOH etching, and **(C, D)** Au/(Si)C after gold loading and calcination.

peaks at 2θ of 44.2° and 51.5° appeared, corresponding to the Co (111) and (200) crystal faces (PDF#15-0806) (Bai et al., 2019). Moreover, after thermal treatment in Ar, no CoO_x phase was detected, suggesting the full self-reduction of Co^{2+} in the high-temperature Ar atmosphere. After NaOH etching, the diffraction peaks of Co were greatly weakened and broadened. Co_3O_4 was observed at 2θ of 31.3°, 36.9°, 38.6°, 59.5°, and 65.3°, relating to the (220), (311), (222), (511), and (440) crystal planes of Co_3O_4 (PDF#76-1802), likely due to the re-oxidation of metallic Co exposed to both the strong basic solution and air. After gold loading and thermal calcination, all diffraction peaks broadened, suggesting the possible re-dispersion of metal species in the Au/(Si)C sample before and after calcination.

Typical SEM images (Figures 1B–E) also revealed the changes in morphology during synthesis. The SiO_2@ZIF prepared in the presence of silica spheres displayed irregular morphology, different from the commonly reported dodecahedron structure of ZIF-67 (Saliba et al., 2018). Small silica spheres were surrounded or inserted on the flat carbon blocks, forming a hybrid composition. After thermal treatment in Ar, the main structure shrank and surface spherical bulging was maintained in the SiO_2@ZIF-Ar. After NaOH etching, the removal of silica from the (Si)C-NaOH was evidenced by the weakened contrast of the spherical shells.

An additional Au/(Si')C sample supported by 350 nm silica spheres (Supplementary Figure S1) was also synthesized for comparison. However, SEM images of the SiO_2(350nm)@ZIF showed phase separation of the ZIF structure from silica (Supplementary Figure S2), mainly caused by the incompatibility of the large spheres. In addition, large Au diffraction peaks were observed in the sample. The sharp diffraction peaks of CoO_x were also observed in the Au/(Si')C (Figure 1A). Thus, the Au/(Si)C and Au/(Si')C synthesized using silica spheres with different diameters greatly influenced the crystallization of metal particles. Stöber silica may act as a structure promoter and enhance the surface distribution of both Au and CoO_x, but only with the proper diameter.

TEM images of SiO_2@ZIF-Ar and (Si)C-NaOH are shown in Figures 2A and B. Combined with the CoO_x diffraction peaks in XRD, the black spots in these images could be ascribed to the co-existence of CoO_x particles after NaOH etching, as denoted by the dotted circles. However, it was surprising that the average particle size was much smaller: only 4.1 nm after Au loading and calcination of the Au/(Si)C. The CoO_x may have been re-dispersed during the etching and calcination process in the presence of Au nanoparticles, consistent with the broadened peaks in the XRD patterns. We observed no metal aggregates in the final Au/(Si)C. Small metal particles with an interplanar distance of 0.235 nm related to the Au (111) crystal plane (Luo et al., 2019) confirmed the surface distribution of the Au particles. The irregular sheet-like carbon structure (arrows in Figures 2C and D) was ascribed to the destroyed multilayer carbon shells after silica etching. The fine dispersion and re-arrangement of the metal species during calcination provided more possibilities to

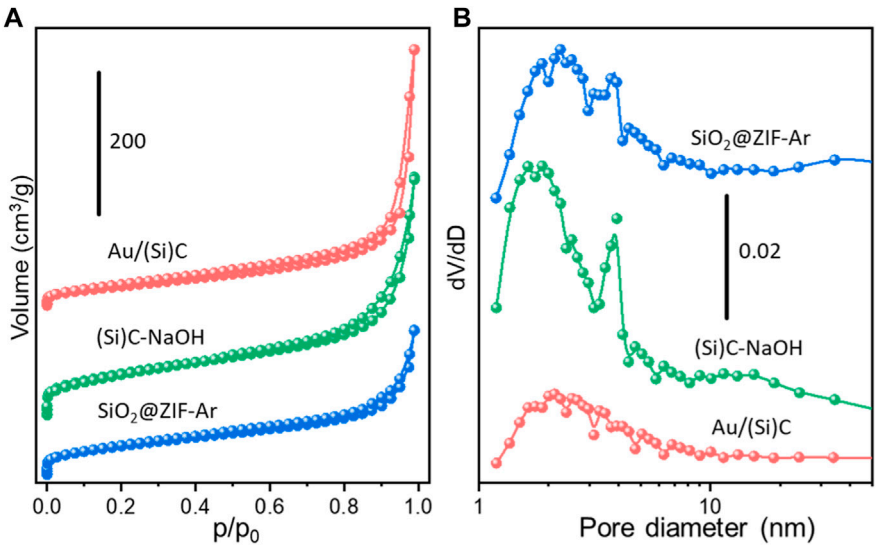

FIGURE 3
(A) N_2 adsorption-desorption isotherms and **(B)** pore diameter distribution of SiO_2@ZIF-Ar after N_2 thermal treatment, (Si)C-NaOH after NaOH etching and Au/(Si)C after gold loading and calcination.

construct new interfaces between Au particles and $Co^{\delta+}$ species in oxidative states, as revealed by their much-broadened XRD diffraction peaks.

Stöber silica was used as a hard template to promote a structure with better texture properties and diffusion effects for liquid-phase reactions. N_2 adsorption-desorption curves were studied to understand the porosity modified by the hard template. Figure 3 shows the isotherm profiles of several typical samples during the synthesis and their pore size distributions. All the tested samples displayed Type IV isotherms exhibiting a small H1 hysteresis loop, corresponding to the existence of mesopores (Zhao et al., 2019). The sharp increase at low p/p_0 (<0.1) confirmed the co-existence of micropores (Li et al., 2018). The pore sizes were in the range of 1–10 nm with mesopores dominating in each sample. The etching process caused an increase in the surface area from 152.8 m^2/g in SiO_2@ZIF-Ar to 216.7 m^2/g in (Si)C-NaOH, with the volume greatly increasing to 0.57 cm^3/g in the latter sample (Supplementary Table S1). The subsequent loading of Au nanoparticles and calcination resulted in pore shrinkage or blockage by Au particles, with the surface area decreasing to 110.1 m^2/g in Au/(Si)C (Yan et al., 2018).

XPS spectra of the (Si)C-NaOH support and the final Au/(Si)C samples were analyzed to understand their surface composition and the possible metal interactions in the gold catalyst. Spectra of the Au 4*f* core level are shown in Figure 4A. The characteristic peaks of Au 4*f*7/2 can be deconvoluted into two peaks at 84.3 eV and 85.5 eV, corresponding to surface Au^0 and $Au^{\delta+}$ species, respectively (Luo J. J. et al., 2022). The binding energy of Au^0 in the Au/(Si)C shifted to a slightly higher value compared to the standard value in the literature (84.0 eV), which is commonly ascribed to electron transfer induced by metal-support synergy (Duan et al., 2020). The surface $Au^{\delta+}$ species reached 16% in the Au/(Si)C, which is reportedly beneficial for many selective oxidation processes (Luo et al., 2017).

The XPS spectra of the Co 2*p* core level suggested the presence of both Co^{3+} and Co^{2+} species with binding energies of 780.2 and 782.1 eV, respectively, in both the (Si)C-NaOH support and Au/(Si)C (Wei et al., 2021). After gold loading and calcination, the percentage of Co^{3+} decreased slightly from 55% to 51% (Supplementary Table S2). Considering the clear peak shift of Au^0 toward a higher binding energy and the generation of $Au^{\delta+}$ species, Au likely specifically interacted with CoO_x on the support, especially neighboring fine CoO_x. Metallic Co^0 species was not present in the tested samples, consistent with the XRD patterns. For better elucidation, O 1*s* spectra were also obtained (Figure 4C). The single broad peak was deconvoluted into three peaks at 530.0, 531.5, and 533.5 eV, which were related to the presence of lattice oxygen species in the metal oxide, oxygenated groups (C=O) on the carbon materials, and adsorbed –OH on the surface (Dong et al., 2020). The percentages of oxygen species (Supplementary Table S2) suggested the promoted formation of lattice oxygen in the Au/(Si)C sample, mostly provided by reducible CoO_x on the surface according to the XRD patterns. Surface lattice oxygen is frequently reported to contribute to the activation and supplementation of active oxygen species during oxidation (Ha et al., 2018). Considering the XRD and the XPS spectra, these findings suggest possible metal interactions and electron delivery between Au and CoO_x-doped carbon. After calcination, both the Au nanoparticles and CoO_x were redispersed on the carbon surface with abundant $Au^{\delta+}$ and lattice oxygen species at a reasonable efficiency for the selective oxidation of alcohol.

The catalytic performances for alkali-free benzyl alcohol (BnOH) oxidation by different catalysts are shown in Figure 5. The as-synthesized Au/(Si)C successfully transformed BnOH at only 80 °C in the absence of alkali with 40.3% conversion. The selectivity of benzaldehyde (BzH) reached 90.4% with a yield of 36.4%. Pure carbon materials (e.g., activated carbon and carbon nanotubes) did not display any detectable activity in the absence of alkali. Au/ZIF and Au/CoO_x, without any structure promotion by Stöber silica, showed BnOH conversion rates as low as 28.5% and 22.3%, respectively, with poor yields toward BzH and other by-products such as toluene. Pure CoO_x–supported Au, the ZIF-67–supported gold, or the (Si)C-NaOH without gold loading did not perform as efficiently as the Au/(Si)C catalyst. The co-existing CoO_x species also affect active Au/(Si)C. We further treated the Au/(Si)C with an aqueous HCl solution to eliminate

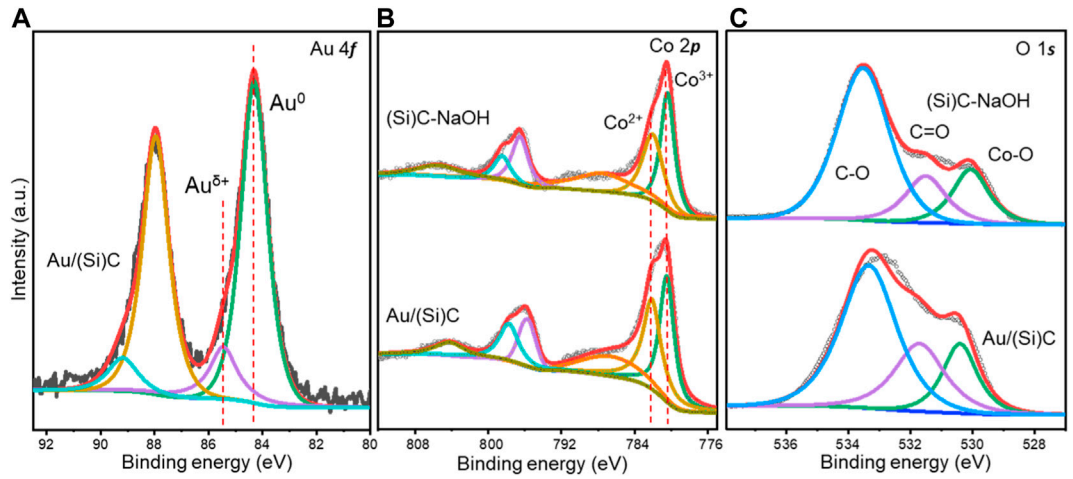

FIGURE 4
XPS spectra of the **(A)** Au 4*f*, **(B)** Co 2*p*, and **(C)** O 1*s* core levels of (Si)C-NaOH after NaOH etching and Au/(Si)C with gold loading.

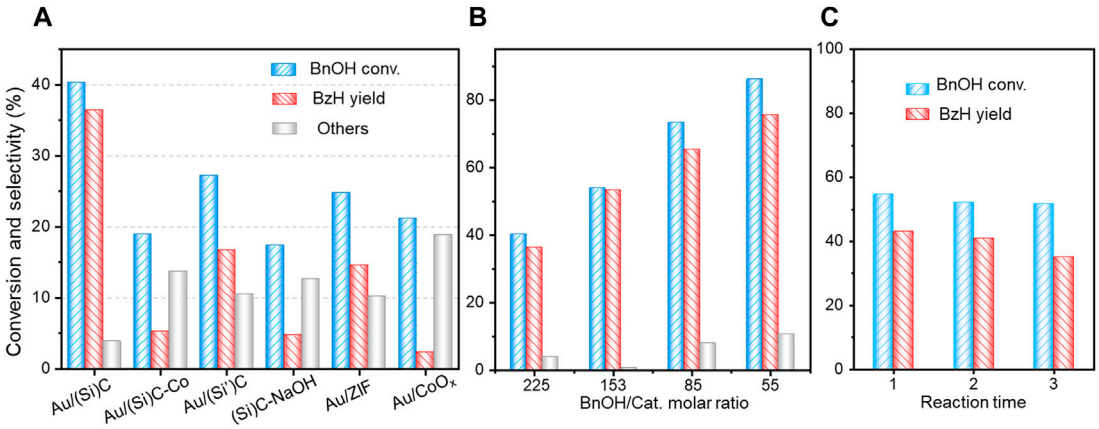

FIGURE 5
(A) Catalytic performances of alkali-free BnOH oxidation *via* the derived Au/(Si)C and different references. **(B)** BnOH conversion as a function of reaction time. **(C)** Stability test of Au/(Si)C. Reaction conditions: A BnOH/Au molar ratio of 225 with 30 mg catalyst was used in **(A)** for better comparison (20 ml/min O_2 flow, 80 °C for 4 h). A BnOH/Au molar ratio of 486 with 7 mg catalyst was used in **(C)** to understand the catalytic stability under limited catalyst dosage. (Si)C-NaOH:SiO_2@ZIF-Ar after NaOH etching to remove the silica template; Au/(Si)C:(Si)C-NaOH with gold loading after calcination at 300 °C for 3 h; Au/(Si')C: a similar sample using silica with 350 nm spheres; Au/(Si)C(-Co):Au/(Si)C etched with HCl to remove Co species; Au/ZIF:ZIF-67–supported Au; Au/CoO_x: CoO_x powder–supported Au particles. 'Others': other by-products in the reaction, primarily toluene.

the influence of CoO_x; however, after CoO_x removal, the Au/(Si)C-Co only showed 19.2% BnOH conversion, illustrating the hindered catalytic process in the absence of CoO_x. The catalytic behavior of Au/(Si)C was greatly enhanced after structure promotion. The promoted structure of Au/(Si)C with finely dispersed metal species and modulated Au-support synergy demonstrated more significant effects on the catalytic performances.

The appropriate hard template for Au/(Si)C is 90 nm Stöber silica; however, the template diameter also requires consideration. Using 350 nm Stöber silica resulted in poor activity with only 27.1% BnOH conversion by Au/(Si')C. The similar BnOH conversion of the Au/ZIF (without template) suggested the lack of usefulness of large silica spheres in Au/(Si')C, mainly due to the incompatibility of such spheres with the ZIF-67 structure in the Au/(Si)C precursor, as shown in Supplementary Figure S2. Consequently, the XPS spectra showed no clear peak shift of Au^0 (Supplementary Figure S4) and only a few lattice oxygen contributed by CoO_x.

The superior catalytic behavior of Au/(Si)C can be viewed as the combined result of the synergy between metals and the promoted structure. The former was reflected by the XPS and XRD results, with metal re-dispersion during synthesis and peak shifts with electron transfer from Au to the support. The fine dispersion of CoO_x on the surface was also revealed by the large amounts of lattice oxygen species, which could help activate and supplement the active oxygen species during BnOH oxidation. The largely promoted mesoporous structure caused by the etching of silica spheres created channels for reactant transportation and diffusion with faster reaction rates. After optimizing the reaction conditions, the alkali-free conversion of BnOH reached approximately

89.3% with a BzH yield of 74.5% at only 80 °C, if the BnOH/Au ratio was kept at 55 for economic reasons (Figure 5B). The catalyst was generally stable, with consistent catalytic performance (Figure 5C) for at least three reaction cycles without post-treatment after drying.

4 Conclusion

We synthesized a series of modified Co-ZIF-67 materials with tunable morphology to support fine Au nanoparticles for the aerobic oxidation of benzyl alcohol. Structure promotion was performed using Stöber silica as a hard template, which was removed by NaOH etching before gold immobilization. The texture structure of Au/(Si)C was greatly improved and revealed by the increased surface area and volume. Consequently, CoO_x was introduced into the carbon shell during the formation of the Co-ZIF-67 precursor. XRD, XPS, and TEM images demonstrated the redispersion of both Au and CoO_x as well as the electronic delivery between metals due to bimetallic synergy. Analysis of the chemical and surface composition suggested a surface rich in $Au^{\delta+}$ with abundant lattice oxygen, which benefited the transformation rate of benzyl alcohol even in alkali-free conditions. The Au/(Si)C with finely dispersed Au particles showed excellent reactivity in the alkali-free environment, with 89.3% benzyl conversion and 74.5% benzaldehyde yield at only 80 °C.

Data availability statement

The original contributions presented in the study are included in the article/Supplementary Material. Further inquiries can be directed to the corresponding authors.

Author contributions

JL and CL contributed to the study conception and design. ZD and SZ organized the database and wrote the manuscript draft. SZ, SY, and WY performed the statistical analyses. All authors contributed to the manuscript revision and read and approved the submitted version.

Conflict of interest

The authors declare that the research was conducted in the absence of any commercial or financial relationships that could be construed as a potential conflict of interest.

Publisher's note

All claims expressed in this article are solely those of the authors and do not necessarily represent those of their affiliated organizations, or those of the publisher, the editors, and the reviewers. Any product that may be evaluated in this article, or claim that may be made by its manufacturer, is not guaranteed or endorsed by the publisher.

Supplementary material

The Supplementary Material for this article can be found online at: https://www.frontiersin.org/articles/10.3389/fceng.2022.1116366/full#supplementary-material

References

Adnan, R. H., and Golovko, V. B. (2019). Benzyl alcohol oxidation using gold catalysts derived from Au8 clusters on TiO_2. *Catal. Lett.* 149, 449–455. doi:10.1007/s10562-018-2625-8

Bai, Y. R., Dong, J. P., Hou, Y. Q., Guo, Y. P., Liu, Y. J., Li, Y. L., et al. (2019). Co_3O_4@PC derived from ZIF-67 as an efficient catalyst for the selective catalytic reduction of NO_x with NH_3 at low temperature. *Chem. Eng. J.* 361, 703–712. doi:10.1016/j.cej.2018.12.109

CáNEPA, A. L., ElíAS, V. R., Vaschetti, V. M., Sabre, E. V., Eimer, G. A., and Casuscelli, S. G. (2017). Selective oxidation of benzyl alcohol through eco-friendly processes using mesoporous V-MCM-41, Fe-MCM-41 and Co-MCM-41 materials. *Appl. Catal. A General* 545, 72–78. doi:10.1016/j.apcata.2017.07.039

Chen, X., Peng, M., Cai, X., Chen, Y., Jia, Z., Deng, Y., et al. (2021). Regulating coordination number in atomically dispersed Pt species on defect-rich graphene for n-butane dehydrogenation reaction. *Nat. Commun.* 12, 2664. doi:10.1038/s41467-021-22948-w

Chen, Y., Guo, Z., Chen, T., and Yang, Y. (2010). Surface-functionalized TUD-1 mesoporous molecular sieve supported palladium for solvent-free aerobic oxidation of benzyl alcohol. *J. Catal.* 275, 11–24. doi:10.1016/j.jcat.2010.07.006

Dong, Y. N., Luo, J. J., Li, S. J., and Liang, C. H. (2020). CeO_2 decorated Au/CNT catalyst with constructed Au-CeO_2 interfaces for benzyl alcohol oxidation. *Catal. Commun.* 133, 105843. doi:10.1016/j.catcom.2019.105843

Duan, D., Hao, C. X., He, G. G., Wang, H. Y., Shi, W. Y., Gao, L. M., et al. (2020). Co_3O_4 nanosheet/Au nanoparticle/CeO_2 nanorod composites as catalysts for CO oxidation at room temperature. *ACS Appl. Nano Mater.* 3, 12416–12426. doi:10.1021/acsanm.0c02922

Feng, J., He, Y., Liu, Y., Du, Y., and Li, D. (2015). Supported catalysts based on layered double hydroxides for catalytic oxidation and hydrogenation: General functionality and promising application prospects. *Chem. Soc. Rev.* 44, 5291–5319. doi:10.1039/c5cs00268k

Ferraz, C. P., Garcia, M. A. S., Teixeira-Neto, É., and Rossi, L. M. (2016). Oxidation of benzyl alcohol catalyzed by gold nanoparticles under alkaline conditions: Weak vs. strong bases. *RSC Adv.* 6, 25279–25285. doi:10.1039/c6ra01795a

Guo, Z., Liu, B., Zhang, Q., Deng, W., Wang, Y., and Yang, Y. (2014). Recent advances in heterogeneous selective oxidation catalysis for sustainable chemistry. *Chem. Soc. Rev.* 43, 3480–3524. doi:10.1039/c3cs60282f

Ha, H., Yoon, S., An, K., and Kim, H. Y. (2018). Catalytic CO oxidation over Au nanoparticles supported on CeO_2 nanocrystals: Effect of the Au-CeO_2 interface. *ACS Catal.* 8, 11491–11501. doi:10.1021/acscatal.8b03539

Jia, Z., Qin, X., Chen, Y., Cai, X., Gao, Z., Peng, M., et al. (2022). Fully-exposed Pt-Fe cluster for efficient preferential oxidation of CO towards hydrogen purification. *Nat. Commun.* 13, 6798. doi:10.1038/s41467-022-34674-y

Li, L., Sun, L., Cang, H., Chu, W., Shao, J. L., and Yan, J. L. (2018). Silica-assisted mesoporous Co@Carbon nanoplates derived from ZIF-67 crystals and their enhanced catalytic activity. *J. Solid State Chem.* 267, 134–139. doi:10.1016/j.jssc.2018.08.019

Liu, L., Zhou, X., Yan, Y., Zhou, J., Zhang, W., and Tai, X. (2018). Bimetallic gold-silver nanoparticles supported on zeolitic imidazolate framework-8 as highly active heterogenous catalysts for selective oxidation of benzyl alcohol into benzaldehyde. *Polymers* 10, 1089. doi:10.3390/polym10101089

Lu, G., Chu, F., Huang, X., Li, Y., Liang, K., and Wang, G. (2022). Recent advances in Metal-Organic Frameworks-based materials for photocatalytic selective oxidation. *Coord. Chem. Rev.* 450, 214240. doi:10.1016/j.ccr.2021.214240

Luo, J., Chu, W., Sall, S., and Petit, C. (2013). Facile synthesis of monodispersed Au nanoparticles-coated on Stöber silica. *Colloids Surfaces A Physicochem. Eng. Aspects* 425, 83–91. doi:10.1016/j.colsurfa.2013.02.056

Luo, J., Dong, Y., Yang, S., Shan, F., Jiang, Q., Ma, Y., et al. (2022a). Au nanoparticles anchored on sulfonated carbon nanotubes for benzyl alcohol oxidation. *ACS Appl. Nano Mater.* 5, 4887–4895. doi:10.1021/acsanm.1c04453

Luo, J. J., Liu, Y. F., Niu, Y. M., Jiang, Q., Huang, R., Zhang, B. S., et al. (2017). Insight into the chemical adsorption properties of CO molecules supported on Au or Cu and hybridized Au-CuO nanoparticles. *Nanoscale* 9, 15033–15043. doi:10.1039/c7nr06018a

Luo, J. J., Liu, Y. F., Zhang, L. Y., Ren, Y. J., Miao, S., Zhang, B. S., et al. (2019). Atomic-scale observation of bimetallic Au-CuO_x nanoparticles and their interfaces for activation of CO molecules. *Acs Appl. Mater. Interfaces* 11, 35468–35478. doi:10.1021/acsami.9b12017

Luo, J. J., Shan, F. X., Yang, S. H., Zhou, Y. X., and Liang, C. H. (2022). Boosting the catalytic behavior and stability of a gold catalyst with structure regulated by ceria. *RSC Adv.* 12, 1384–1392. doi:10.1039/d1ra07686h

Luo, J., Shan, F., Yang, S., Zhou, Y., and Liang, C. (2022b). Boosting the catalytic behavior and stability of a gold catalyst with structure regulated by ceria. *RSC Adv.* 12, 1384–1392. doi:10.1039/d1ra07686h

Parmeggiani, C., Matassini, C., and Cardona, F. (2017). A step forward towards sustainable aerobic alcohol oxidation: New and revised catalysts based on transition metals on solid supports. *Green Chem.* 19, 2030–2050. doi:10.1039/c7gc00406k

Saliba, D., Ammar, M., Rammal, M., Al-Ghoul, M., and Hmadeh, M. (2018). Crystal growth of ZIF-8, ZIF-67, and their mixed-metal derivatives. *J. Am. Chem. Soc.* 140, 1812–1823. doi:10.1021/jacs.7b11589

Su, F.-Z., Liu, Y.-M., Wang, L.-C., Cao, Y., He, H.-Y., and Fan, K.-N. (2008). Ga–Al mixed-oxide-supported gold nanoparticles with enhanced activity for aerobic alcohol oxidation. *Angew. Chem. Int. Ed.* 47, 334–337. doi:10.1002/anie.200704370

Tang, C., Zhang, N., Shao, Q., Huang, X., and Xiao, X. (2019). Rational design of ordered Pd–Pb nanocubes as highly active, selective and durable catalysts for solvent-free benzyl alcohol oxidation. *Nanoscale* 11, 5145–5150. doi:10.1039/c8nr07789d

Wang, T., Yuan, X., Li, S., Zeng, L., and Gong, J. (2015). CeO_2-modified Au@SBA-15 nanocatalysts for liquid-phase selective oxidation of benzyl alcohol. *Nanoscale* 7, 7593–7602. doi:10.1039/c5nr00246j

Wei, X. J., Barkaoui, S., Chen, J. W., Cao, G. P., Wu, Z. Y., Wang, F., et al. (2021). Investigation of Au/Co_3O_4 nanocomposites in glycol oxidation by tailoring Co_3O_4 morphology. *Nanoscale Adv.* 3, 1741–1746. doi:10.1039/d1na00053e

Xu, Y., Li, J., Zhou, J., Liu, Y., Wei, Z., and Zhang, H. (2020). Layered double hydroxides supported atomically precise Aun nanoclusters for air oxidation of benzyl alcohol: Effects of size and active site structure. *J. Catal.* 389, 409–420. doi:10.1016/j.jcat.2020.06.017

Yan, R., Zhao, Y., Yang, H., Kang, X. J., Wang, C., Wen, L. L., et al. (2018). Ultrasmall Au nanoparticles embedded in 2D mixed-ligand metal-organic framework nanosheets exhibiting highly efficient and size-selective catalysis. *Adv. Funct. Mater.* 281, 1802021. doi:10.1002/adfm.201802021

Yu, X., Huo, Y., Yang, J., Chang, S., Ma, Y., and Huang, W. (2013). Reduced graphene oxide supported Au nanoparticles as an efficient catalyst for aerobic oxidation of benzyl alcohol. *Appl. Surf. Sci.* 280, 450–455. doi:10.1016/j.apsusc.2013.05.008

Zhao, T. T., Hui, Y. J., Niamatullahand Li, Z. H. (2019). Controllable preparation of ZIF-67 derived catalyst for CO_2 methanation. *Mol. Catal.* 474, 110421. doi:10.1016/j.mcat.2019.110421

Zhou, H. J., Zheng, M. B., Tang, H., Xu, B. Y., Tang, Y., and Pang, H. (2020). Amorphous intermediate derivative from ZIF-67 and its outstanding electrocatalytic activity. *Small* 16, 1904252. doi:10.1002/smll.201904252

Zhu, J., Wang, P. C., and Lu, M. (2014). Selective oxidation of benzyl alcohol under solvent-free condition with gold nanoparticles encapsulated in metal-organic framework. *Appl. Catal. A General* 477, 125–131. doi:10.1016/j.apcata.2014.03.013